Acquisition of Complete Acoustic Emission Amplitude Records during Rock Fracture Experiments

S.D. Goodfellow[1], J.W. Flynn[2], J.M. Reyes-Montes[2], M.H.B. Nasseri[1] and R.P. Young[1]
[1] Department of Civil Engineering, University of Toronto, Toronto, Canada
[2] Applied Seismology Consultants, Shrewsbury, United Kingdom

Abstract

This paper presents the results from a triaxial deformation experiment where acoustic emission (AE) waveforms were continuously recorded at two different gain levels. The purpose of this work is to quantify the extent of missing amplitude data, which is typically lost at critical points during rock fracture experiments due to waveform clipping. A cylindrical sample of Westerly granite was axially loaded until failure at a constant displacement rate and 25 MPa of confining pressure. AE was monitored by 18 piezoelectric sensors mounted on the cylinder ends and around its circumference. AE data was continuously acquired and digitized at 10 MHz and 12-bits for the duration of the experiment where four channels were amplified 6 dB and the rest 40 dB. Two large stress-drops occurred in the post peak-stress regime resulting in large amplitude bursts of AE. Channels amplified 40 dB showed complete amplitude saturation, making event analysis difficult whereas those channels amplified 6 dB remained unclipped. We conclude that the amount of missing amplitude data is significant for experiments of this nature and should be considered when designing AE acquisition setups.

1. Introduction

Acoustic emission (AE) monitoring is a technique used to monitor damage accumulation in engineering structures and brittle materials under load. When local stress conditions, at the micro scale, reach a critical level, fractures will form and release energy, some of which is in the form of elastic waves. To study the failure process of different materials under controlled conditions, laboratory experiments are conducted under different loading conditions. A common experiment in experimental rock mechanics is the triaxial deformation test. In this experiment, a cylindrical rock sample is brought to a hydrostatic stress using steel loading platen on the cylinder ends and silicone oil via a rubber sleeve. From this point, the rock is loaded to failure by compressing the rock along the cylinder axis at a constant displacement rate. In the post peak-stress regime, stored elastic energy in the rock and steel platens forces fractures to propagate dynamically leading to catastrophic failure.

At the time of catastrophic failure, AE is difficult to analyze because the acquisition system saturates. Schubnel et al. [1] studied fluid-induced rupture of Fontainebleau sandstone during triaxial deformation experiments. During dynamic fault propagation, they assumed the period of full waveform saturation (5 ms) was related to the rupture time, which provided an upper bound for the rupture velocity of 4 m/s. Thompson et al. [2] studied the failure of intact rock using a continuous AE acquisition system. Channels used to source locate events were amplified 40 dB. As the sample approached failure, the waveform amplitude significantly increased, resulting in a 95 ms period prior to failure where no AE locations could be obtained. Additionally, amplitude saturation can cause issues when calculating frequency-magnitude statistics.

Lei et al. [3-7] solved this problem by using two acquisition systems during their experiments. A full waveform recorder, capable of switching between triggered and continuous modes, was used to record waveforms, which were used for source location and mechanism analysis.

Channels hooked up to the full waveform recorder were amplified by 40 dB. Maximum waveform amplitudes from two AE transducers were recorded on a separate acquisition unit with 99 dB dynamic range.

Recently, an effort has been made to bridge the gap between AE produced during mm scale laboratory rock fracture experiments and larger natural earthquakes by using quantitative seismology theory [8, 9]. For this type of analysis, unclipped amplitude records of the complete AE catalogue are essential for studying events over a wide range of magnitudes.

In this paper we study AE produced during dynamic failure of rock specimens, which was amplified at two different levels. By studying unclipped waveforms at the time of catastrophic failure, we hope to gain insight into the nature of waveforms acoustically radiated during dynamic rupture propagation.

2. Experimental Procedure And Data Acquisition

2.1 Sample Preparation

Westerly granite was chosen because it has been extensively studied and is well suited to AE studies [2] because of its homogeneous and isotropic structure. The mean grain size is 0.75 mm and modal analyses give the following mineralogical composition in volumetric percent:
quartz 27 %, microcline 36 %, plagioclase 30 %, phyllosilicates 6 % and others 1 % [10].

A cylindrical sample 125 mm in length and 50 mm in diameter was prepared conforming to the 2.5 length/diameter aspect ratio recommended by the International Society of Rock Mechanics (ISRM, 1977 [11]). The sample was prepared using a hollow coring drill, and its end faces were ground and polished to within 0.01 mm parallelism using a diamond CNC grinding wheel. After the sample was machined to the specifications mentioned above, it was thermally treated in a high-temperature oven to induce micro-fractures along grain boundaries. The sample was heated to a temperature of 850^{o}C, at a rate of 2^{o}C/min. In this experiment, the reason for thermally damaging the rock was to promote a more controlled failure to maximize the number of recorded AE waveforms. Lei et al. [3] reported that pre-existing cracks are the most dominant factor of all heterogeneities that govern fault nucleation in laboratory rock fracture experiments.

2.2 Triaxial Deformation Cell

A triaxial deformation cell (ErgoTech Ltd.) equipped to handle a cylindrical rock specimen was used to conduct the reported experiment (Fig. 1). The axial load was applied by an external hydraulic actuator (MTS) operated under displacement control and the confining pressure was delivered via silicone oil and a rubber jacket. Two pairs of orthogonal cantilevers were used to measure diametral strain, while a pair of LVDTs measured axial strain. The cell is equipped with 18 piezoelectric sensors for monitoring AE activity. The AE sensors (designed by Laszlo Lombos, formerly of ErgoTech Ltd.) are sensitive to surface normal velocity and were calibrated between 100 kHz and 1.4 MHz using a laser interferometer [12]. Three AE sensors are located in each loading platen (spring loaded) and the other 12 are embedded in the rubber confining jacket (Fig. 1). AE sensors have a contact area diameter of 3 mm. Three additional pairs of ultrasonic sensors for contemporaneous measurements of P, S_1 and S_2 waves are located along three orthogonal axes.

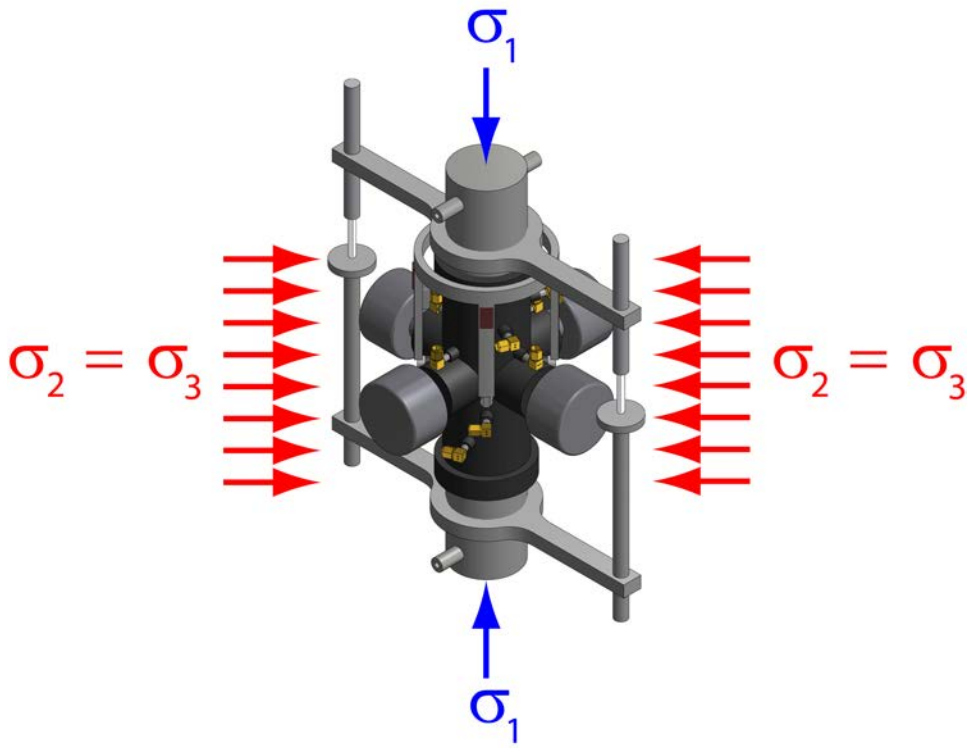

Fig. 1: Triaxial geophysical imaging cell.

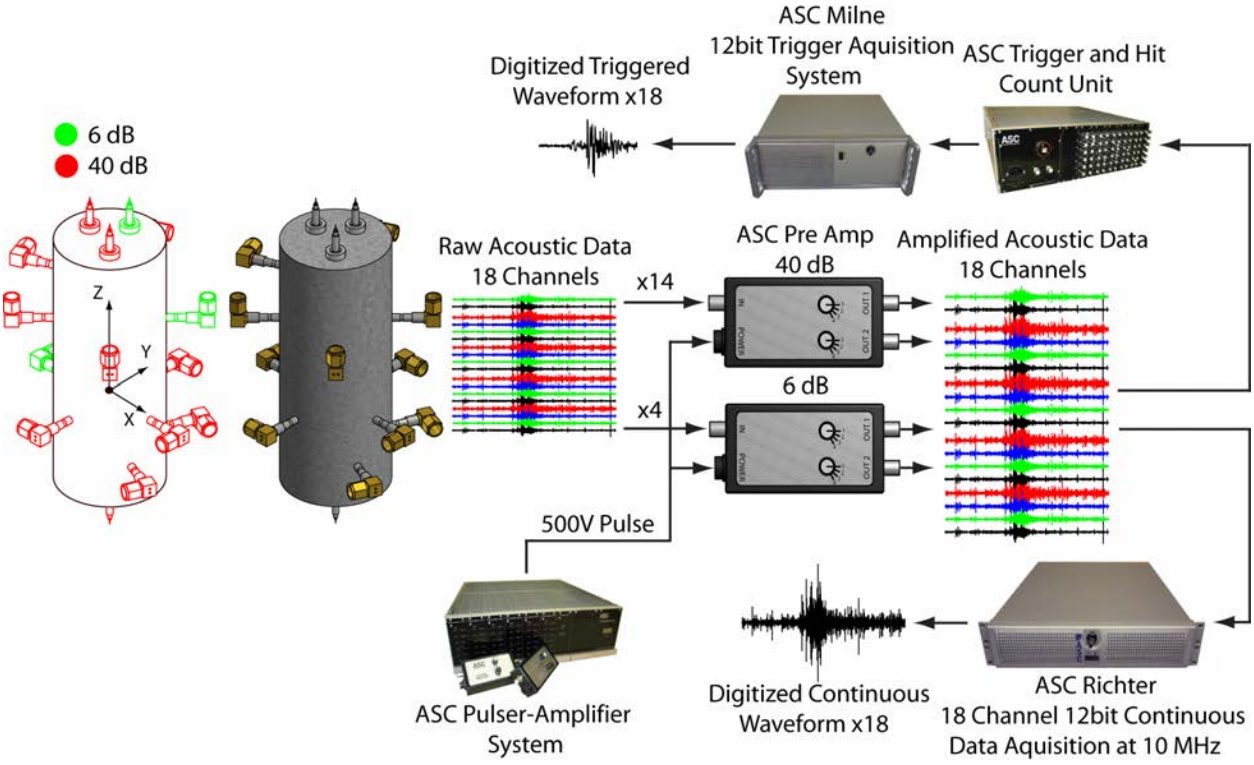

Fig. 2: Acoustic Emission acquisition setup.

2.3 Acoustic Emission Data Acquisition

AE signals were amplified using Applied Seismology Consultants (ASC) preamplifiers, which include a 100 kHz – 1 MHz band-pass filter module in each unit. Data from 18 AE

sensors was acquired continuously at a sampling rate of 10 MHz and 12-bit resolution using the ASC Richter system. Typically with 40 dB amplification, less than a second before brittle failure the acquisition system saturates resulting in clipped waveforms. In an attempt to acquire full, unclipped waveforms during failure of the specimen, some channels had their amplification reduced. During the reported experiment, raw AE signals on 14 channels (Fig. 2) were amplified by 40 dB and the remaining 4 channels were amplified by 6 dB. After the experiment, the continuous AE waveforms were harvested to extract discrete events. A trigger was defined at four channels recording a voltage of more than 80 mV (i.e. threshold voltage) within a window length of 512 sample points (51.2 μs). If this criterion was met, a waveform length of 1,024 sample points for each channel was written to file.

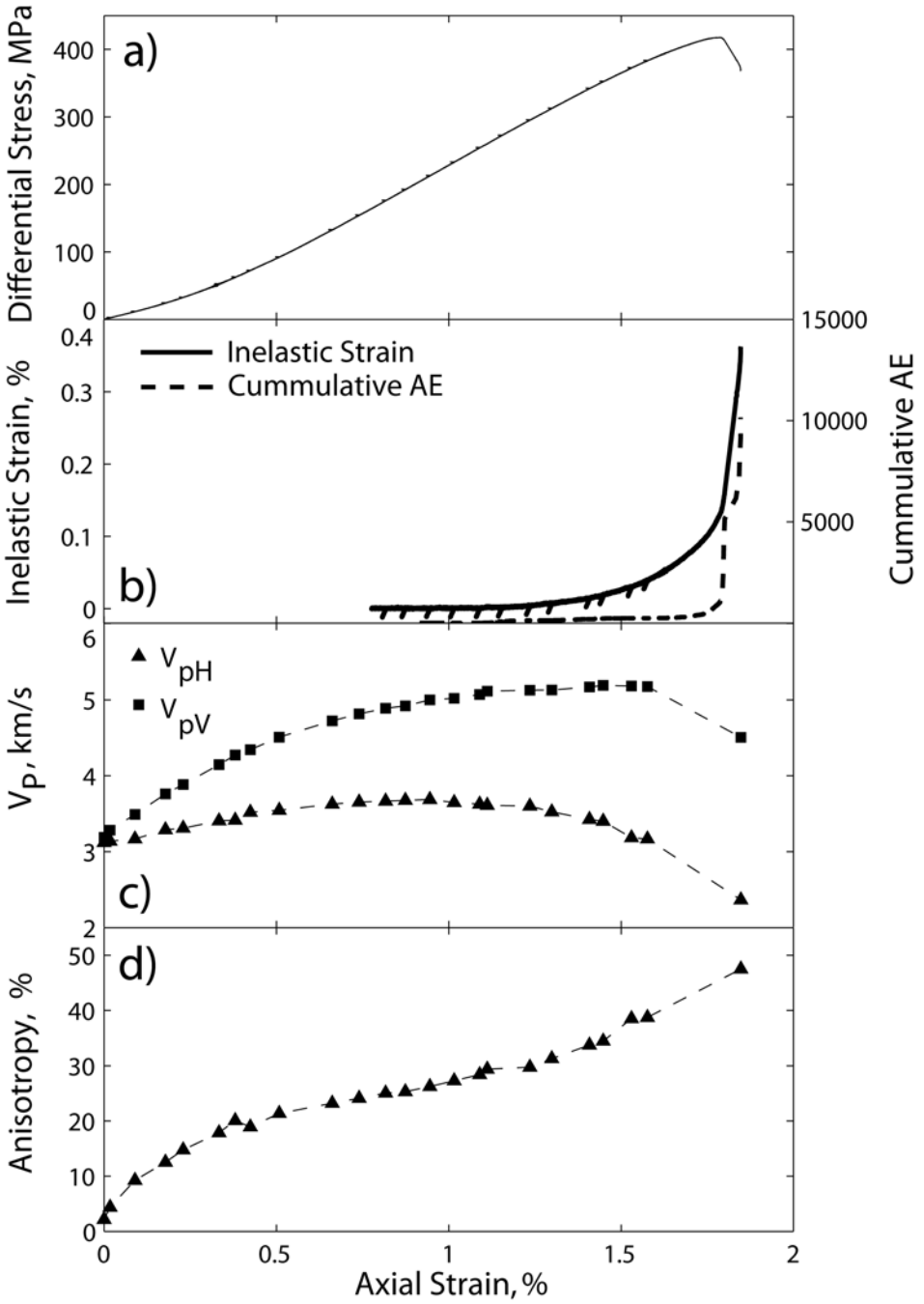

Fig. 3: a) Differential stress, b) inelastic strain and AE count, c) P-wave velocity and d) P-wave velocity anisotropy.

3 Results

3.1 Basic Analysis

The sample was loaded hydrostatically to 25 MPa and then differentially until failure at a constant displacement rate of 0.2 μm/s. In Fig. 3a the differential stress is plotted against axial strain up until just before final failure. The initial portion of the stress-strain curve shows plastic deformation caused by the closing of grain boundary micro-cracks, which were induced during heating. Once the micro-cracks were closed, the rock responded linearly to continued axial shortening. Figure 3b displays the inelastic strain and cumulative AE counts. The stress-strain curve diverged from linearity at a differential stress and axial strain of approximately 256 MPa and 1.1% respectively. AE signals began to appear as the inelastic strain started to increase. Cumulative AE reached a maximum value of 10,000 counts before final failure. In Fig. 3c the axial (V_{pV}) and lateral (V_{pH}) P-wave velocities are plotted against axial strain. The axial P-wave velocity gradually increased during the pre-failure measurement period whereas the lateral velocity started to decrease at a point that roughly coincided with initiation of inelastic strain and sample dilation. The difference in axial and lateral velocity trends is caused by the creation of micro-fractures aligned parallel to σ_1. Figure 3d presents the P-wave velocity anisotropy, which is the percentage difference between the axial and lateral P-wave velocities. P-wave velocity anisotropy was roughly 0 % at a hydrostatic stress of 25 MPa and increased steadily to almost 50 % after final failure.

3.2 Continuous Acoustic Emission Waveforms

In Figs. 4a and 4b, differential stress and AE waveform amplitude from channel 16, amplified at 40 dB, are plotted against loading time for the last 3,600 s and 200 s of the experiment, respectively. After peak stress, there were two stress drops (SD1 and SD2), which were separated by roughly 18 s. The first stress drop was 30 MPa and the second was 305 MPa. Leading up to SD1, the waveform amplitude ramped up and the ±5 V dynamic range of the acquisition system was saturated almost continuously for 18 s between stress drops. Figure 4c displays the waveform amplitude for Channel 17, which was amplified at 6 dB, for a 45-s interval spanning both stress drops. With the lower amplification level, the acquisition system did not saturate during dynamic failure.

3.3 Acoustic Emission Hypocenter Locations

P-wave arrivals were automatically picked and event hypocenter locations were calculated using the downhill Simplex method. We were able to locate 4,357 events from roughly 20,000 triggers harvested from the continuous waveforms. The majority of AE events occurred between the last two velocity surveys, during which time the axial P-wave velocity decreases from 5,174 m/s to 4,506 m/s and the anisotropy increases from 38.76% to 57.5%. To improve the source location accuracy, a time varying velocity model was employed.

AE source locations were divided into four time bins and are plotted in Figs. 4d - 4k. Two faults were induced during sample failure and are highlighted in red and blue where the red fault was induced during SD1 and the blue fault during SD2. Nucleation began in the upper left side at the sample's edge and lasted for roughly 5 seconds before SD1. Coinciding with SD1, a cloud of AE locations propagates rapidly towards the bottom of the sample. There is a small gap in AE locations (green line), which is a result of cascading micro-fracture events that occurred in such close succession and such large amplitudes that individual events could not be easily identified.

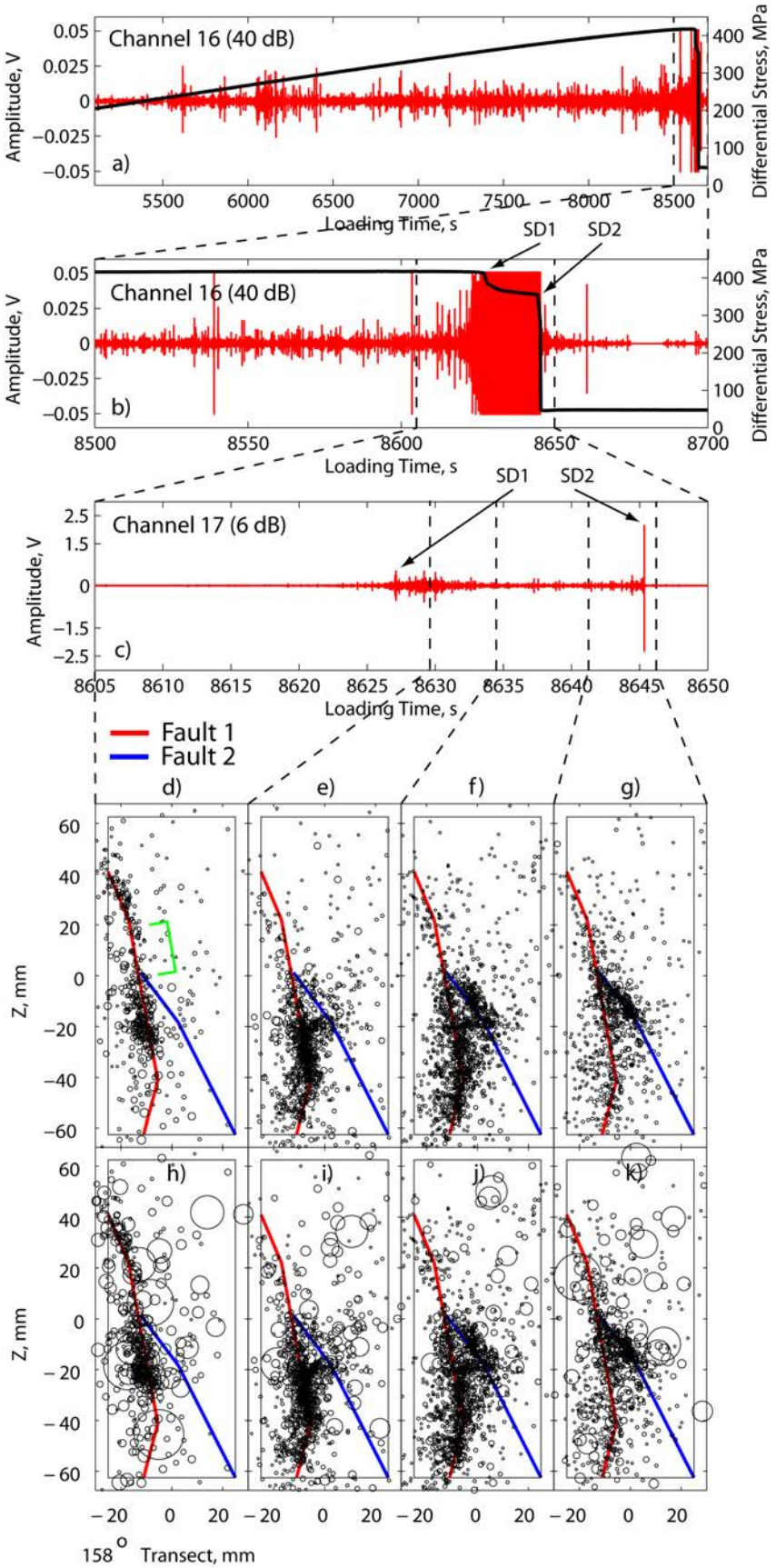

Fig. 4: a, b) Channel 16 waveform (40 dB) and differential stress, c) Channel 17 waveform (6 dB), d-g) AE source locations scaled to the maximum amplitude recorded on the 40-dB channels, h-k) AE source locations scaled to the maximum amplitude recorded on the 6-dB channels.

In Figs. 4d – 4g, event locations are represented by black circles whose radii were scaled to the maximum recorded amplitude on the 40 dB channels. This means that the event radii were scaled by voltages ranging from ±0.4 mV (noise floor) to ±0.05 V (saturation level of the acquisition system at 40-dB amplification). In Figs. 4h – 4k, radii were scaled to the maximum recorded amplitude from either the 40-dB or 6-dB channels, meaning radii were scaled by voltages ranging from ±0.4 mV (noise floor of the 40-dB channels) to ±2.5 V (saturation level of the acquisition system at 6-dB amplification).

4 Discussion

In Figs. 4h – 4k, we scaled event radii by the combined maximum recorded amplitude from the 40-dB and 6-dB channels. Visualization of the complete amplitude record presents new perspectives for studying the unstable failure process of geo-materials. Figure 4h shows the rapid propagation of the first fault, which produced a number of events with significantly larger amplitudes than the majority. Additionally, large amplitude events appear to be located on portions of the fault where there were no dense clouds of smaller amplitude events. This suggests that the large amplitude events are associated with the rapid propagation of fractures or coalescence of previously induced micro-fractures.

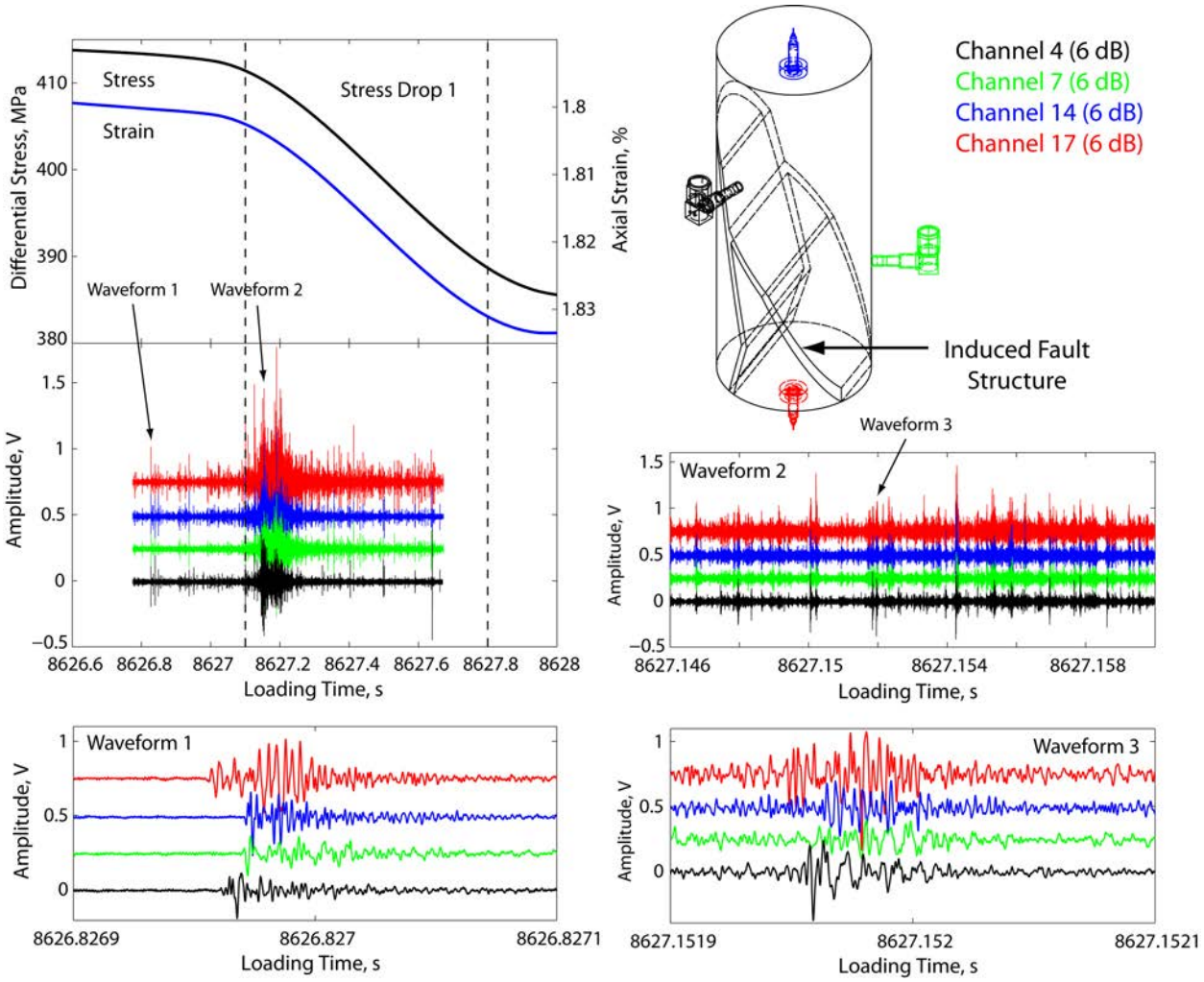

Fig. 5: Continuous AE waveforms from channels 4, 7, 14, and 17, amplified 6 dB during SD1 including the sensor locations.

Figure 5 presents differential stress and axial strain plotted against loading time for SD1. At this critical point, channels amplified 40 dB are completely saturated making identification of discrete events difficult. Included in Fig. 5 is a diagram of the rock sample with the 6-dB sensor locations and geometry of the induced fault structure. In Figure 5, waveforms from channels 4, 7, 14, and 17, amplified 6 dB, show no sign of saturation during SD1. During the height of fracturing, the waveform appears as a quick succession of discrete large amplitude waveforms superimposed on a background of micro-fracturing noise.

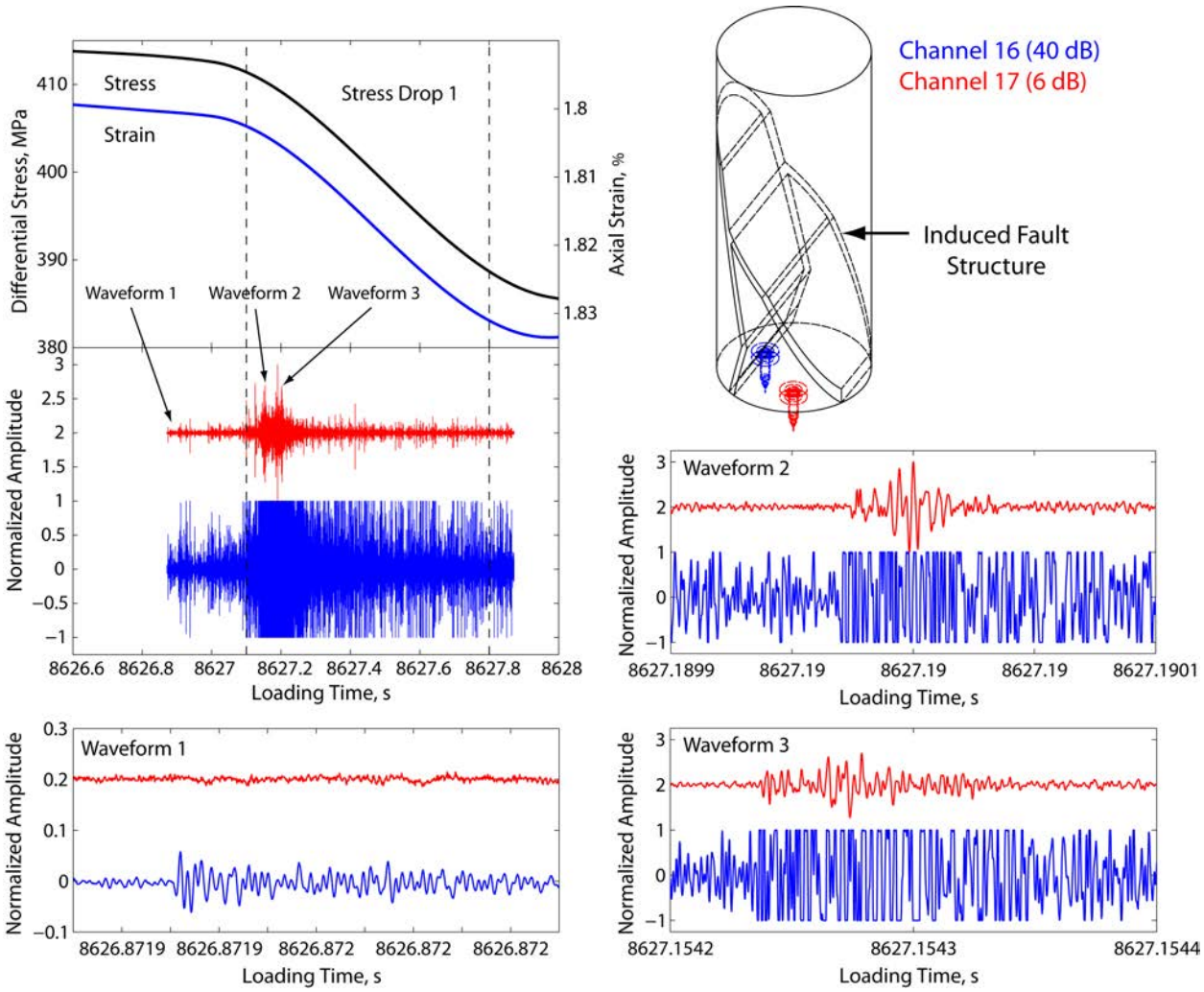

Fig. 6: Continuous AE waveforms from channels amplified by 40 dB and 6 dB (16 and 17) during SD1 including the sensor locations.

Waveforms from channel 16 (40 dB) and channel 17 (6 dB) are presented in Fig. 6. AE sensors connected to channels 16 and 17 are located next to each other on the bottom loading platen and therefore the amplitude of incident wave fronts should be approximately the same. Waveform 1 was recorded 0.2 seconds before SD1 and shows good signal to noise ratio (SNR) on channel 17 (40 dB) whereas no waveform is recorded on channel 16 (6 dB). During SD1, waveforms 2 and 3 show clipped signals on channel 16 and clear discrete waveforms on channel 17.

The results presented above show two distinct amplitude regimes. In the first regime, AE activity is produced by grain scale micro-fracturing. This regime continues through nucleation, coalescence and quasi-static fault propagation right up until the point of instability. In the second

regime, the fault propagated dynamically producing large amplitude waveforms in rapid succession. Figure 7 shows channel 16 (40 dB) waveform superimposed on channel 17 waveform. Waveform 1 occurred during the first regime where channel 16 recorded a multitude of small amplitude events with good SNR. Channel 17 shows a coarse resolution with low SNR and most of the small amplitude waveforms buried in the noise. Waveform 2 occurred during the second regime where channel 16 is almost continuously saturated but channel 17 displayed full, unclipped waveforms. These results highlight the need for multi-scale acquisition during rock fracture experiments.

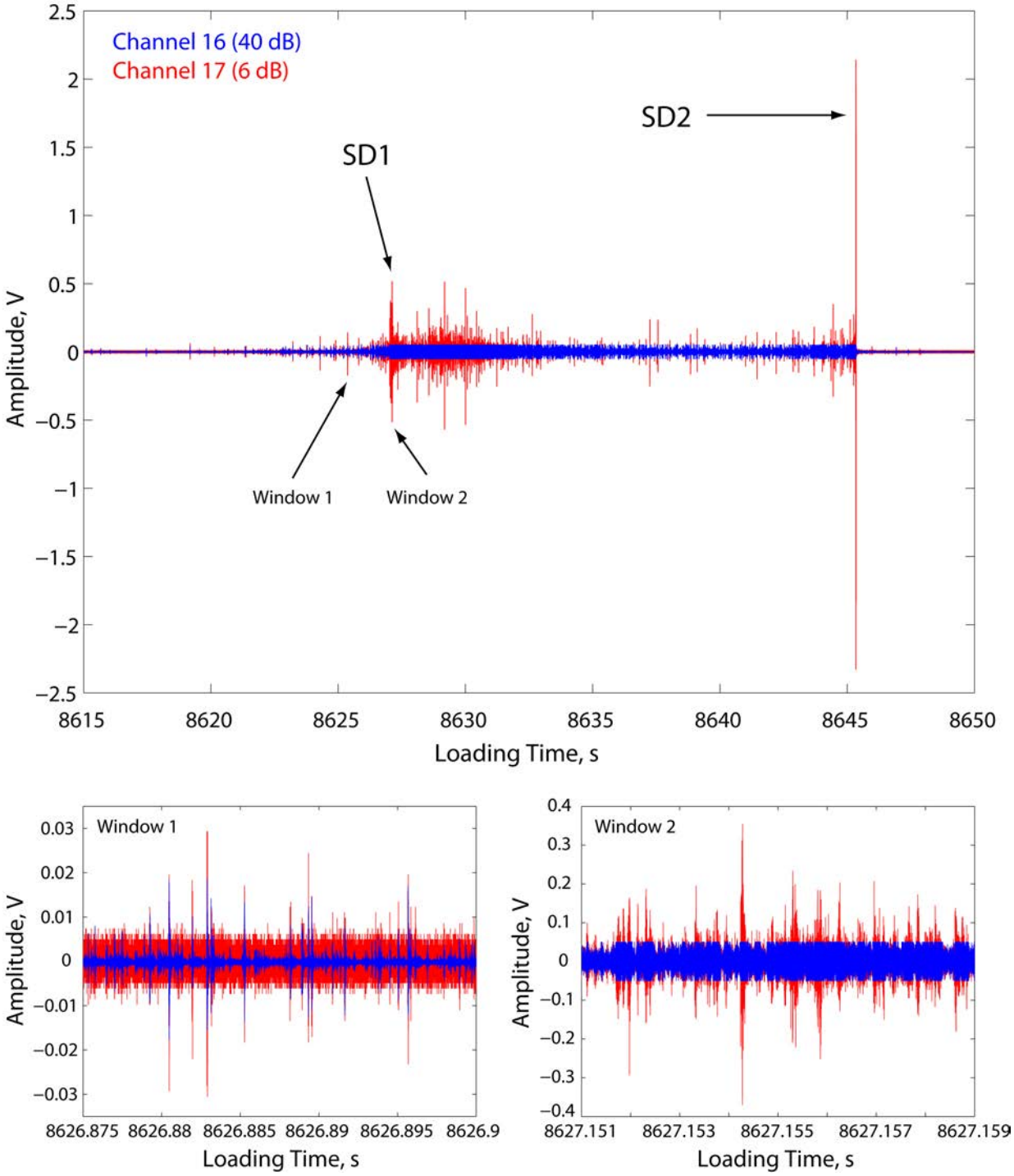

Fig. 7: Continuous AE waveforms from channels 16 and 17 superimposed on each other for 35 seconds spanning SD 1 and SD2.

5 Conclusion

In this paper we presented the results from a triaxial deformation experiment on a cylindrical sample of high-temperature-treated Westerly granite. AE data from 18 sensors was continuously digitized at 10 MHz and 12-bits resolution for the duration of the experiment. 14 channels were amplified 40 dB and the remaining 4 were amplified 6 dB. Approximately 20,000 events were harvested from the continuous waveforms and a time-varying velocity model was used to determine the source locations of 4,357 events. Analysis of AE locations showed the growth of an initial fracture that arrested on the bottom loading platen, and was followed by the growth of a second fracture resulting in the final 305 MPa stress drop.

Analysis of continuous waveforms from 40-dB and 6-dB channels demonstrated a wide range of waveform amplitudes. Amplitudes ranged from ±0.4 mV (noise floor of the 40-dB channels) to ±2.5 V (saturation level of the acquisition system at 6-dB amplification). We identified two regimes of fracturing: (1) micro-fracturing produced during nucleation and quasi-static fault propagation, which generated small amplitude waveforms and (2) dynamic fault propagation producing large amplitude waveforms. Typically in rock fracture experiments, the data acquisition setup is optimized to capture waveforms from the first regime, which is used to track the spatial evolution of damage. We showed that by reducing amplification during the second regime, discrete unclipped waveforms can be recorded and analyzed bringing new information about the failure process of rock under elevated stress.

Acknowledgements

We would like to thank Laszlo Lombos and Applied Seismology Consultants for their technical support. The funding for the creation and operation of the Rock Fracture Dynamics Facility at the University of Toronto was provided by the Canada Foundation for Innovation and the Province of Ontario (Grant no. 0000302419) and the Natural Sciences and Engineering Research Council of Canada (Grant no. 0000300001), respectively.

References

1. B.D. Thompson, R.P. Young, D.A. Lockner (2006), Fracture in Westerly granite under AE feedback and constant strain rate loading: Nucleation, Quasi-static propagation, and the transition to unstable fracture propagation, Pure and Applied Geophysics, **163**, 995-1019.
2. A. Schubnel, B.D. Thompson, J. Fortin, Y. Gueguen, R.P. Young (2007), Fluid-induced rupture experiment on Fontainebleau sandstone: Premonitory activity, rupture propagation, and aftershocks, Geophysical Research Letters, **34**, L19307.
3. X. Lei, K. Kusunose, O. Nishizawa, A. Cho, T. Satoh (2000), On the spatio-temporal distribution of acoustic emissions in two granitic rocks under triaxial compression: the role of pre-existing cracks, Geophysical Research Letters, **27**, 1997-2000.
4. X. Lei, K. Masuda, O. Nishizawa, L. Jouniaux, L. Liu, W. Ma, T. Satoh, K. Kusunose (2004), Detailed analysis of acoustic emission activity during catastrophic fracture of faults in rock, Journal of Structural Geology, **26**, 247- 258.
5. X. Lei (2003), How do asperities fracture? An experimental study of unbroken asperities, Earth and Planetary science letter, **213**, 347-359.
6. X. Lei, K. Masuda, T. Satoh, O. Nishizawa (2003), The hierarchical rupture process of a fault: an experimental study, Physics of the Earth and Planetary Interiors, **137**, 213-228.

7. X. Lei, K. Kusunose (2000), Quasi-static fault growth and cracking in homogeneous brittle rock under triaxial compression using acoustic emission monitoring, Journal of Geophysical Research, **105**, 6127-6139.
8. E.J. Sellers, M. O. Kataka, and L. M. Linzer (2003), Source parameters of acoustic emission events and scaling with mininginduced seismicity, J. Geophys. Res., **108**, B9 2418.
9. G.C. McLaskey, B. D. Kilgore, D. A. Lockner, and N. M. Beeler (2014), Laboratory generated M -6 earthquakes, Pure Appl. Geophys., **31**, 157-168.
10. M.H.B. Nasseri, A. Schubnel, P.M. Benson, R.P. Young (2009), Common evolution of mechanical and transport properties in thermally cracked Westerly granite at elevated hydrostatic pressure, Pure and Applied Geophysics, **166**, 927-948.
11. ISRM suggested method for determining uniaxial compressive strength of rock materials, Document No. 1, first revision, 1977.
12. P. Theobald and R. Pocklington (2010), Velocity sensitivity calibration of AE sensors using the through wave method and laser interferometry, EWGAE 2010, Vienna, Austria, September 1-8, 2010.